Electronic and phase stability properties of V–X (X = Pd, Rh, Ru) alloys

2004 J. Phys.: Condens. Matter 16 5615

(http://iopscience.iop.org/0953-8984/16/30/021)

INSTITUTE OF PHYSICS PUBLISHING JOURNAL OF PHYSICS: CONDENSED MATTER

J. Phys.: Condens. Matter **16** (2004) 5615–5630 PII: S0953-8984(04)81212-8

Electronic and phase stability properties of V–X (X = Pd, Rh, Ru) alloys

P E A Turchi[1], R M Waterstrat[2], R Kuentzler[3,5], V Drchal[4] and J Kudrnovský[4]

[1] Lawrence Livermore National Laboratory (L-353), PO Box 808, Livermore, CA 94551, USA
[2] National Institute of Standards and Technology, Gaithersburg, MD 20899-8551, USA
[3] Institut de Physique, CNRS/IPCM, 3 rue de l'Université, F-67084 Strasbourg, France
[4] Institute of Physics, Academy of Sciences of the Czech Republic, Na Slovance 2, CZ-182 21 Praha 8, Czech Republic

Received 24 May 2004
Published 16 July 2004
Online at stacks.iop.org/JPhysCM/16/5615
doi:10.1088/0953-8984/16/30/021

Abstract

In this work, we focus on the ordered structures of V–X systems, where X = Ru, Rh, Pd, and relate the variation in the difference of the numbers of valence electrons of the alloy constituents to the information contained in the constitution phase diagrams, and the electronic and stability properties. The electronic properties deduced from the low-temperature specific heat studies are presented for the V–Ru and V–Rh systems and compared with those of the V–Pd alloys for which new experimental results are also included. The theoretical analysis based on first-principles electronic structure calculations confirms the measured variation of the electronic specific heat coefficients with alloy composition, and predicts specific ordering trends in the V–X systems. The superconducting properties are described for the V–X disordered alloys, the ordered $V_{1-x}Rh_x$ and $V_{1-x}Ru_x$ systems, and are related to their structural instability.

1. Introduction

The relationship between electronic properties and stability of ordered alloys has been the subject of a previous study [1] in which the properties of $\tilde{X}$–Pd, where $\tilde{X}$ = V, Nb, Ta, have been compared. In these three systems, a common T_{10} transition metal (Pd) has been combined with three T_5 elements (V, Nb, and Ta) to compare the properties of 'iso-electronic' systems for which the difference in the numbers of valence electrons of the alloy constituents (ΔN) is kept constant. The experimental observations were considered to be in agreement with theoretical band-structure calculations that showed that a pseudo-bandgap splits the d-band into low-energy majority states (Pd) and higher-energy minority states (V, Nb, or Ta). The

[5] Deceased.

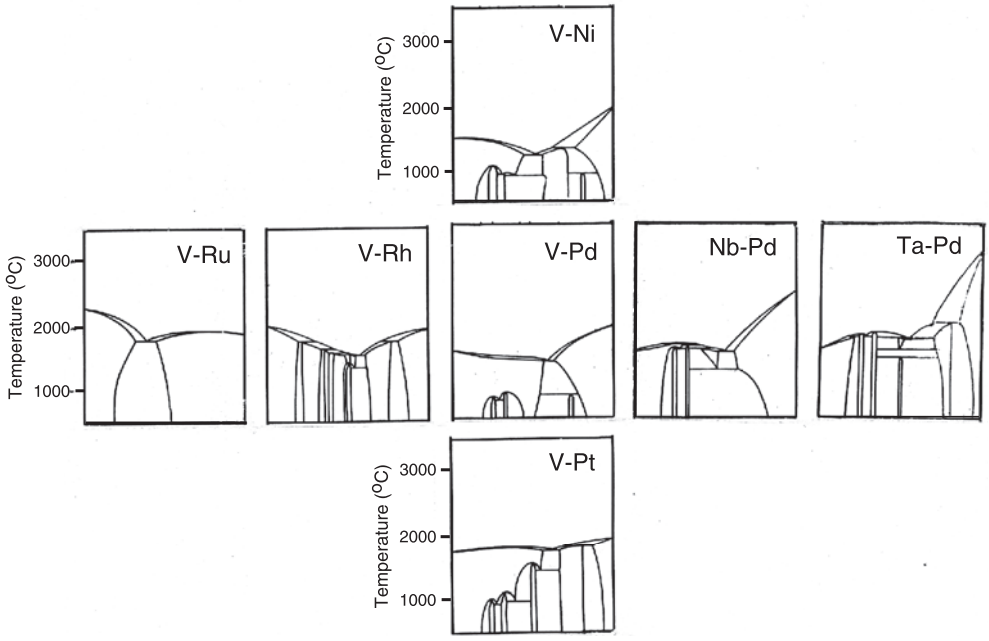

Figure 1. Phase diagrams (from [1–4]) of the V–Ru, V–Rh, and V–Pd systems (horizontal triad from left) compared to the isoelectronic systems V–Ni, V–Pd, and V–Pt (vertical triad), and V–Pd, Nb–Pd, and Ta–Pd (horizontal triad from right) including updated versions of the Ta–Pd [5] and Nb–Pd [1] phase diagrams.

Fermi level, E_F, fell in the pseudo-bandgap or in its vicinity, and this explained the relatively low values of the specific heat coefficients, γ, for the ordered phases as well as a decreasing γ with increasing formation temperature [1].

In the present study we compare the behaviour of the related V–X systems, where X = Ru, Rh, and Pd, in which a common T_5 element (V) is combined with a T_8, T_9, or T_{10} element. In these systems the effects of a steadily increasing electron concentration (or ΔN) can be studied, in contrast to the 'iso-electronic' systems.

The paper is organized as follows. In section 2 we comment on the salient features of the assessed phase diagrams of the three binary alloys. In section 3 we discuss sample preparation and experimental procedures for the measurement of heat capacity and magnetic susceptibility. In section 4 we briefly present the theoretical modelling that is used to describe electronic structure, stability and ordering trends for the three alloys. Then, in section 5 we present the experimental results for the solid solutions and the ordered phases together with their physical interpretation and comments on stability properties and ordering trends before concluding in section 6.

2. Phase diagrams

From the commonly accepted phase diagrams for these three alloys shown in figure 1 [2–4], and in contrast to the 'iso-electronic' systems among which many similarities exist [1], these systems are remarkably different, and there are no compound structures that are common to all three systems. Note that the phase diagrams of Nb–Pd and of an updated version of Ta–Pd [5] are also reported in figure 1 for subsequent discussion.

The phase diagram of the V–Ru system has a deceptively simple description and consists exclusively of the two terminal solid solutions [2]. However, the disordered V-rich solid solution extends only up to about 30 at.% Ru where the bcc structure yields to an ordered B2 (CsCl-type) structure. The nature of this transformation is not well understood. The B2 structure, in turn, extends to about 46 at.% Ru where it starts to become increasingly tetragonal with further addition of Ru. Finally, at about 50 at.% Ru, the tetragonal B2-type structure is replaced by an incommensurate modulated structure [6].

The V–Rh system exhibits at least six intermediate phases formed by peritectic reaction or congruently [3]. From about 22 to 35 at.% V, there exists an ordered phase having the $L1_2$ (Cu_3Au-type) ordered structure. This is followed by an ordered V_3Rh_5 phase stable over a narrow composition range. From about 40 to 48 at.% V, there is an ordered phase having an $L1_0$ (CuAu-type) structure. An ordered phase with about 50 at.% V has the α VIr-type structure. This structure appears to be a distorted version of the B2-type structure. A phase region (α_1) occurs at high temperatures whose structure is not yet determined but which is probably a disconnected Rh-terminal solid solution. Finally an A15 Frank–Kasper phase is stable in the range 63–75 at.% V.

The V–Pd system exhibits rather extensive terminal solid solutions which in the Pd-rich region undergoes two order–disorder transformations to ordered phases having the $D0_{22}$ (Al_3Ti-type) and $C11_b$ ($MoPt_2$-type) chemical configurations. A metastable ordered structure was also reported to occur at equi-atomic composition, and preliminary x-ray analysis suggested a deformed structure of AuCd-type. Finally an incompletely ordered A15-type phase extends from about 71 to 76 at.% V.

The only similarity between the three systems is the existence of an ordered structure around the equi-atomic composition. Once again, this has to be contrasted with the strong similarities that are noted among 'iso-electronic' systems such as V–Ni, V–Pd, and V–Pt, or V–Pd, Nb–Pd, and Ta–Pd, as illustrated in figure 1.

3. Sample preparation and experimental procedures

Our sample preparation procedures have been described in [1], and many of the samples used in this study are the same ones used for the phase diagram studies. This is especially appropriate for systems such as V–Rh for which sample preparation is rather challenging, and problems of oxidation of the alloy constituents, exact composition, and homogenization have always to be faced. The vanadium used in the experiments was 99.95% pure since its physical properties are very much dependent on the impurity content. Annealing treatments are given in tables 1–3. Disordered samples were either water quenched or cold worked. The specific heat measurements were carried out between 1.5 and 10 K using a quasi-adiabatic pulse-heating method with an on-line measuring device [7]. Measurements were made between 1.5 and 20 K for most samples, and occasionally up to 40 K. The precision of the measurements was about 1%. The magnetic susceptibility of a few samples was measured between 100 and 300 K with a translation balance. In every case studied, no magnetic order was detected, i.e., all samples exhibited a paramagnetic behaviour. The specific heat data contained no anomalies as a function of temperature, and were therefore fitted without ambiguity with the usual equation: $C = \gamma T + \beta T^3$, where γ and β are the electronic and lattice coefficients, respectively. These coefficients yield the density of states (DOS) at the Fermi energy, $n(E_F)$, according to

$$\gamma = 2/3\pi^2 k_B^2 n(E_F) \tag{3.1}$$

where k_B is Boltzmann's constant, and the Debye temperature Θ_D is given by

$$\Theta_D = (1.944/\beta)^{1/2}. \tag{3.2}$$

Table 1. Electronic coefficient γ (in mJ/g.at.K), Debye temperature Θ_D (in K), superconducting transition temperature T_c (in K), structure, and heat treatment for V–Ru alloys.

Alloy	γ	Θ_D	T_c	Structure	Heat treatment
V	9.70	379	5.36	bcc	as-cast
$V_{95}Ru_5$	7.30	440	1.70	bcc	1050 °C/2 days
$V_{90}Ru_{10}$	5.90	430	<1	bcc	idem
$V_{85}Ru_{15}$	4.60	500	<1	bcc	idem
$V_{80}Ru_{20}$	2.80	510	<1	bcc	idem
$V_{75}Ru_{25}$	2.03	485	<1	B2	idem
$V_{70}Ru_{30}$	2.05	506	<1	B2	1600 °C/3 h
$V_{69}Ru_{31}$	2.66	558	<1.5	B2	as-cast
$V_{65}Ru_{35}$	2.03	455	<1.5	B2	idem
$V_{60}Ru_{40}$	4.82	495	<1.5	B2	1600 °C/3 h
$V_{57}Ru_{43}$	6.07	480	2.88	B2	1600 °C/24 h
$V_{54}Ru_{46}$	8.12	412	4.90	Tetr.	as-cast
$V_{52.5}Ru_{47.5}$	4.60	430	<1.5	?	as-cast

Table 2. Same as for table 1 for V–Rh alloys.

Alloy	γ	Θ_D	T_c	Structure	Heat treatment
V	9.70	379	5.36	bcc	as-cast
$V_{95}Rh_5$	7.03	378	<1.5	bcc	idem
$V_{90}Rh_{10}$	5.04	387	<1.5	bcc	idem
$V_{75}Rh_{25}$	2.51	485	<1	A15	idem
$V_{69}Rh_{31}$	3.80	450	<1	A15	idem
$V_{65}Rh_{35}$	4.70	480	1.036	A15	750 °C/8 weeks
$V_{50}Rh_{50}$	2.80	500	<1	VIr	1100 °C/3 weeks
$V_{47}Rh_{53}$	3.02	341	<1	$L1_0$	idem
$V_{44}Rh_{56}$	4.20	319	<1	$L1_0$	900 °C/6 weeks
$V_{37.5}Rh_{62.5}$	4.36	428	<1	V_3Rh_5	1400 °C/3 h
$V_{31}Rh_{69}$	4.12	460	<1	$L1_2$	idem
$V_{27.5}Rh_{72.5}$	1.95	490	<1	$L1_2$	idem
$V_{25}Rh_{75}$	1.73	540	<1	$L1_2$	idem
$V_{15}Rh_{85}$	3.30	420	<1	fcc	1100 °C/3 weeks
$V_{10}Rh_{90}$	4.00	474	<1	fcc	idem
V_5Rh_{95}	3.80	490	<1	fcc	idem
Rh	4.70	500	<1	fcc	as-cast

In fact for the superconducting samples (VRu, V_3Rh, and dilute V–X alloys), the true DOS is multiplied by an enhancement factor $(1 + \lambda_{e-ph})$ associated with electron–phonon coupling that can be estimated by the McMillan relation. Additional enhancement is caused by spin fluctuations, λ_{spin}, and this is particularly true for Pd which exhibits the strongest exchange of that sort among the pure metals. However, in the following our data have not been corrected for these enhancement factors.

4. Electronic structure modelling and equilibrium results

For chemically random fcc- and bcc-based V–X alloys, electronic structure calculations were carried out on the basis of the charge self-consistent fully relativistic version of the tight-binding linear muffin-tin orbital coherent potential approximation (TB-LMTO-CPA) method within the atomic sphere approximation (ASA) and the local density approximation (LDA) of

Table 3. Same as for table 1 for V–Pd alloys.

Alloy	γ	Θ_D	T_c	Structure	Heat treatment
V	9.70	379	5.36	bcc	as-cast
$V_{97.5}Pd_{2.5}$	7.50	420	<1.5	bcc	idem
$V_{95}Pd_5$	6.50	440	<1.5	bcc	idem
$V_{90}Pd_{10}$	4.55	450	<1.5	bcc	idem
$V_{85}Pd_{15}$	4.55	385	<1.5	bcc	1400 °C/5 h
$V_{77}Pd_{23}$	4.80	360	<1.5	bcc	idem
$V_{75}Pd_{25}$	5.06	469	<1.5	A15	700 °C/2 months
$V_{73}Pd_{27}$	4.95	339	<1.5	bcc	1400 °C/5 h
$V_{72}Pd_{28}$	5.22	420	<1.5	A15	700 °C/2 months
$V_{71}Pd_{29}$	5.40	393	<1.5	bcc	1400 °C/5 h
$V_{50}Pd_{50}$	5.75	320	<1.5	fcc	idem
$V_{50}Pd_{50}$	4.99	366	<1.5	?	600 °C/2 days
$V_{45}Pd_{55}$	5.50	365	<1.5	fcc	1400 °C/5 days
$V_{40}Pd_{60}$	6.05	315	<1.5	fcc	idem
$V_{33}Pd_{67}$	6.35	360	<1.5	fcc	idem
$V_{33}Pd_{67}$	3.59	388	<1.5	$C11_b$	840 °C/140 h
$V_{30}Pd_{70}$	5.40	335	<1.5	fcc	1400 °C/5 h
$V_{25}Pd_{75}$	5.15	357	<1.5	fcc	idem
$V_{25}Pd_{75}$	3.97	427	<1.5	$D0_{22}$	840 °C/140 h
$V_{23}Pd_{77}$	3.80	395	<1.5	$D0_{22}$	idem
$V_{20}Pd_{80}$	4.45	370	<1.5	fcc	1400 °C/5 h
$V_{15}Pd_{85}$	3.70	350	<1.5	fcc	as-cast
$V_{10}Pd_{90}$	4.00	315	<1.5	fcc	idem
V_5Pd_{95}	5.40	300	<1.5	fcc	idem
V_2Pd_{98}	7.35	275	<1.5	fcc	idem
Pd	9.05	265	<1.5	fcc	idem

density functional theory [8]. The LDA calculations were based on the exchange–correlation energy of Ceperley and Alder [9] as parameterized by Perdew and Zunger [10]. To eliminate the charge transfer effects, at each lattice parameter and alloy composition, the atomic sphere radii of the two species were adjusted in such a way that atoms were charge neutral while preserving the total volume of the alloy. The densities of states were evaluated on a line 0.005 Ryd above the real axis (with an energy step of about 5 mRyd) and then deconvoluted on the real axis. The CPA equations were solved iteratively using the method described in [8]. Ordering trends have been predicted with the generalized perturbation method (GPM) [11, 12] in the context of the TB-LMTO-CPA electronic structure description of the chemically disordered alloys. Within the GPM the ordering part of the total energy for a binary alloy $A_{1-c}B_c$ is given to second order in perturbation by [11–13]

$$\Delta E_{\mathrm{ord}}(\{q_s\}) \simeq \sum_s q_s V_s(c) \tag{4.1}$$

with $q_s = c/2(n_s^{\mathrm{BB}} - cn_s)$, where n_s^{BB} and n_s refer to the number of BB pairs and the total number of pairs per site, respectively, associated with the sth-neighbour shell, and c is the concentration in B species. In this last equation, V_s represents an sth-neighbour effective pair interaction (EPI) given by $V_s = V_s^{\mathrm{AA}} + V_s^{\mathrm{BB}} - 2V_s^{\mathrm{AB}}$. The sign convention is such that when $V_s > 0$ (<0), AB (AA or BB) pairs associated with a species at the origin and the other in the sth-neighbour shell are favoured. Within this formalism, the formation (or mixing) energy of

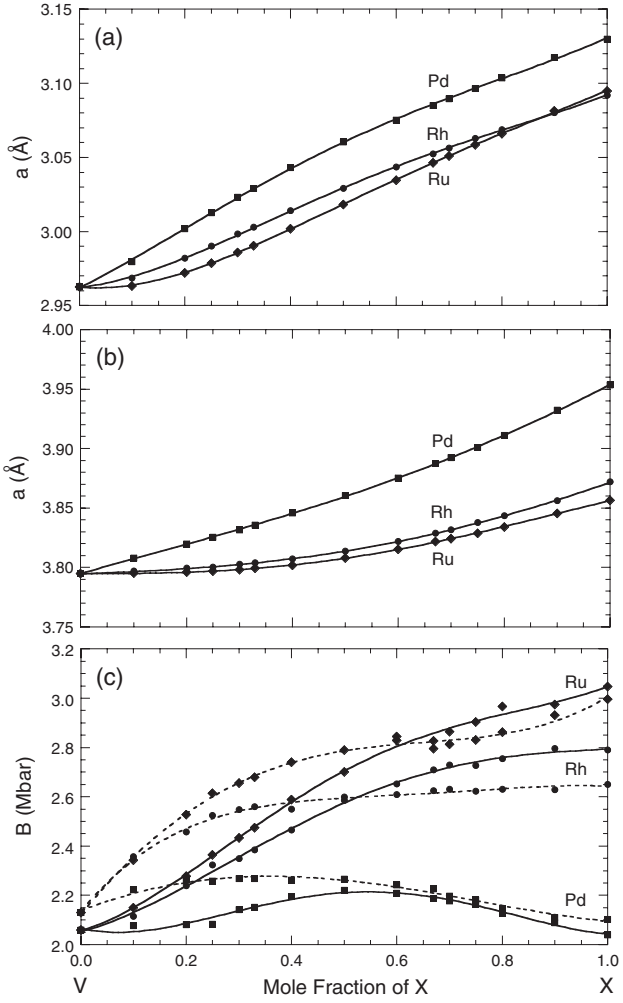

Figure 2. Variation of the lattice constant (in Å) for (a) bcc- and (b) fcc-based alloys, and (c) of the bulk modulus (in Mbar) for bcc- (dashed curve) and fcc-(solid curve) based alloys as functions of composition.

the chemically random alloy is given by

$$\Delta E_{\rm mix}(\{c_i\}) = E^{\rm CPA}_{\rm alloy} - \sum_i c_i E^{\rm eq}_i \tag{4.2}$$

where c_i is the concentration in species i, and $E^{\rm CPA}_{\rm alloy}$ and $E^{\rm eq}_i$ are the energies of the chemically random alloy and of the pure element i, respectively, at their equilibrium lattice parameter, whereas the energy associated with a chemical configuration $\mathcal{C}$ defined by $\{q_s\}$ is written as

$$\Delta E^{\mathcal{C}}(\{q_s\}) = \Delta E_{\rm mix}(\{c_i\}) + \Delta E_{\rm ord}(\{q_s\}). \tag{4.3}$$

Based on TB-LMTO-CPA calculations the equilibrium properties have been obtained for the three alloys based on bcc and fcc lattices, and the results are reported in figure 2 for the lattice parameter and the bulk modulus. As usually observed, the results that correspond to the actually observed structures are within about 1% for the lattice constant and 15% for

the bulk modulus. Note that for the bcc-based disordered alloys, a positive departure from Vegard's law is observed for V–Pd in the entire range of composition and for V–Rh at high Rh composition, whereas for the fcc-based alloys, all three alloys exhibit a negative departure from Vegard's law. Usually, a positive (negative) departure from linearity is associated with a tendency towards phase decomposition (formation). Except for the case of V–Pd, the addition of X = Ru, Rh to a vanadium matrix significantly increases the bulk modulus (and therefore cohesion) independently of the structure (bcc or fcc).

5. Results and discussion

The experimental specific heat was plotted in the usual way, C/T versus T^2, and no anomalies of magnetic or superconductivity origin were observed. The variation of γ and Θ_D with alloy composition is represented in figures 3 and 4, respectively, for the three systems. The values for the V–Pd system are taken from [1, 14] except at low Pd composition for which additional measurements have been carried out for this work (cf table 3). Similarly, in the V–Ru case, the data from Flükiger *et al* [15] at high Ru content have been included. We shall now briefly comment on the experimental results by first considering the disordered alloys, then the ordered phases, and the interplay between order and superconductivity, before presenting the results obtained from first-principles electronic structure calculations.

5.1. Disordered alloys

The disordered states of the three systems present quite similar physical properties, except for the hexagonal phase of V–Ru. The three V-rich solid solutions are characterized by a decrease of γ, an increase of Θ_D, and by the disappearance of superconductivity with an increase in the X component. However, note that the negative slope $d\gamma/dc$, where c is the alloy composition, varies with the nature of the alloy species. The DOS of pure V at the Fermi energy is known to be located in a region of high density. This feature will persist in the disordered alloy, although chemical disorder usually tends to smear out the sharpness of the DOS. Based on the DOS of the pure elements in the bcc and fcc structures calculated with the TB-LMTO methodology, see figure 5, the same general comments can be made. First of all, as is already known, the DOS show features that are characteristics of the underlying lattice, independently of the element considered. Indeed, in the case of bcc-based elements, a typical pseudo-gap that separates bonding from anti-bonding states, mostly of d-character, is observed. The location of the Fermi energy is directly related to the number of valence electrons. Hence, in the case of V, the Fermi energy is located on the left of the pseudo-gap in a region of high electron density, whereas for the other three elements, the Fermi energy is on the right of the pseudo-gap also in a region of high density except for Pd. In the case of the fcc-based elements, the Fermi energy is located in a region of high density for both V and Pd, whereas for Ru and Rh E_F is in a relatively flat region of DOS. Ignoring alloying effects, the addition of solute with a higher number of valence electrons (or higher Fermi energy) to a bcc matrix of pure V will result in a sharp decrease of the DOS at E_F, and therefore of γ. Similarly, since the Fermi energy of the Pd DOS is also located in a region of high density as pointed out in previous studies (see, e.g., [16]), the addition of vanadium to the fcc matrix will lead to a significant decrease in the DOS at E_F, and therefore of γ.

Calculations of the DOS, using the TB-LMTO-CPA method, have been performed as functions of composition for the three chemically random alloys based on the bcc and fcc lattices. We show in figure 6 the DOS for bcc-based V_3X and fcc-based VX_3 alloys. As expected, the partial DOS of V is located at higher energy than the one associated with X.

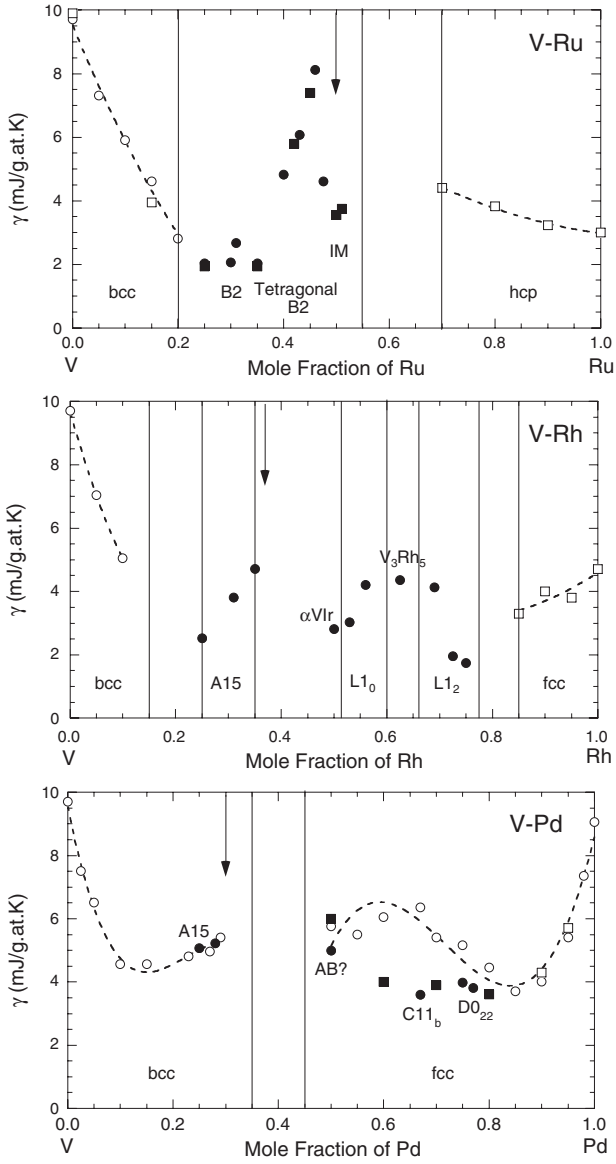

Figure 3. Variation of the coefficient of electronic specific heat γ versus alloy composition for the V–Ru, V–Rh, and V–Pd systems. Open (closed) circles denote disordered (ordered) phases. The squares refer to the data from [14, 15] for V–Pd and V–Ru, respectively. Vertical lines show the approximate composition ranges of each phase. For each alloy, the vertical arrowed line indicates the composition associated with $e/a = 6.5$.

Disorder effects tend to wash out the fine details of the DOS although the overall shape of the partial DOS is similar to the one associated with the corresponding pure element. Since Ru is the closest to V, the alloying effect is less pronounced, and a pseudo-gap is still observed in the bcc case. From Ru to Rh and Pd, the difference in the electron scattering properties with vanadium increases and this is reflected in the shape of the fcc DOS that becomes more and more featureless. The results of $n(E_F)$ reported in figure 7 are directly comparable to the

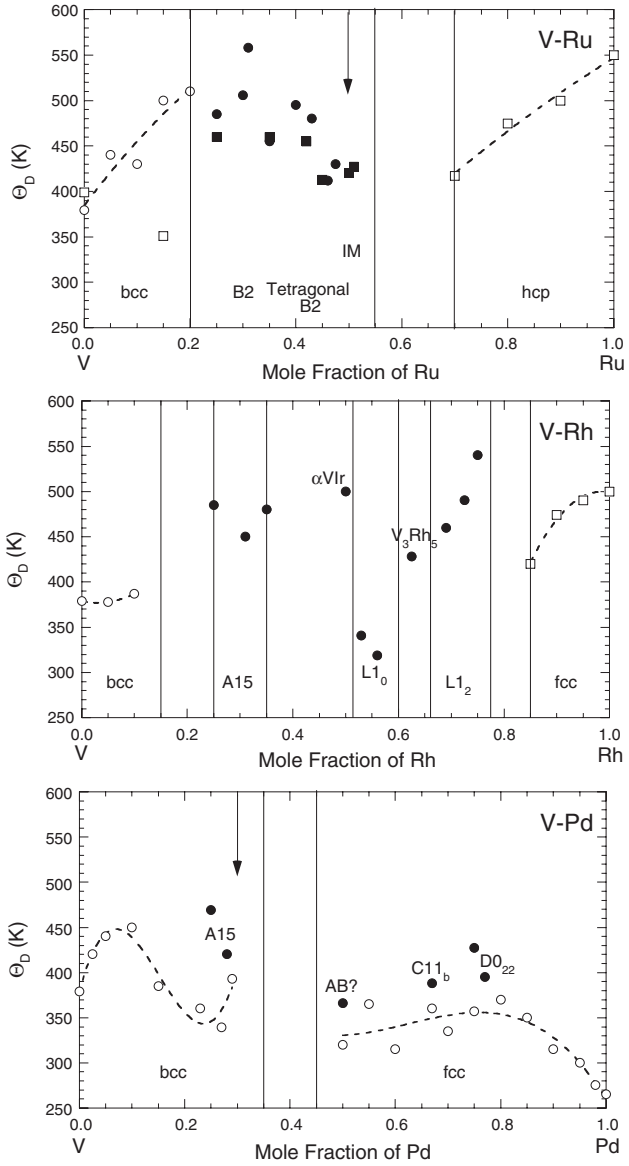

Figure 4. Variation of the Debye temperature, Θ_D, with alloy composition for the V–Ru, V–Rh, and V–Pd systems.

experimentally determined values of γ shown in figure 3. In the region where the ground-state structure is experimentally observed (either bcc or fcc), the agreement is excellent. In all three alloy cases a sharp decrease of $n(E_F)$, or γ, is observed at low vanadium content. On the other hand, for the dilute vanadium-solid solutions, X–V (X = Ru, Rh, Pd), with an increase in the vanadium composition, a sharp decrease of $n(E_F)$ for Pd, a slight decrease for Rh, and finally a slight increase for Ru are predicted, compatible with what is observed experimentally, although in the case of Ru the ground-state structure is hcp and not fcc. Once again, since the d-band of Pd is completely below the Fermi level, see figure 5, and E_F is located in a region of

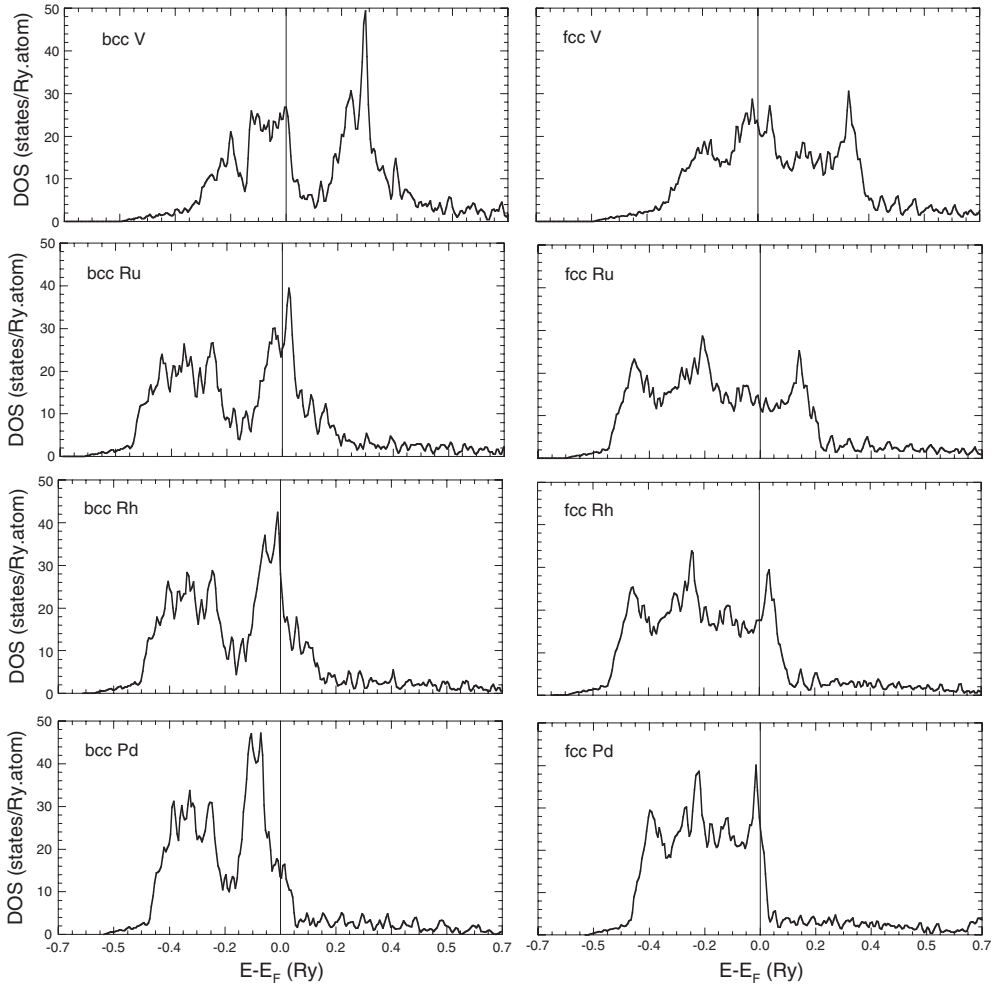

Figure 5. DOS of the pure elements based on the bcc (left panels) and fcc (right panels) structures.

high DOS, an abrupt change of γ and χ can be expected when the impurity d-level comes close to the Pd d-band so that most of the anti-bonding states are also occupied. This is particularly the case for V impurities in a Pd matrix, as observed experimentally. Nevertheless, to compare quantitatively the predicted values of DOS at the Fermi energy to experimental results, the enhancement factor λ must in principle be accounted for.

It should be noted that there is a qualitative agreement between the evolution with alloy composition of the experimentally deduced Debye temperature, Θ_D, cf figure 4, and the calculated bulk modulus, B, cf figure 2. In particular, for bcc-based V-rich alloys, both quantities exhibit a positive slope with alloy composition, whereas at low V composition, the sign of the slope changes from negative (for Ru–V) to positive (for Pd–V). These observations simply confirm the fact that both quantities are a good measure of the degree of cohesion in the condensed matter.

The superconducting property is a periodic function of the valence electron per atom ratio, (e/a), and this is reflected in our experimental results since e/a increases when one considers

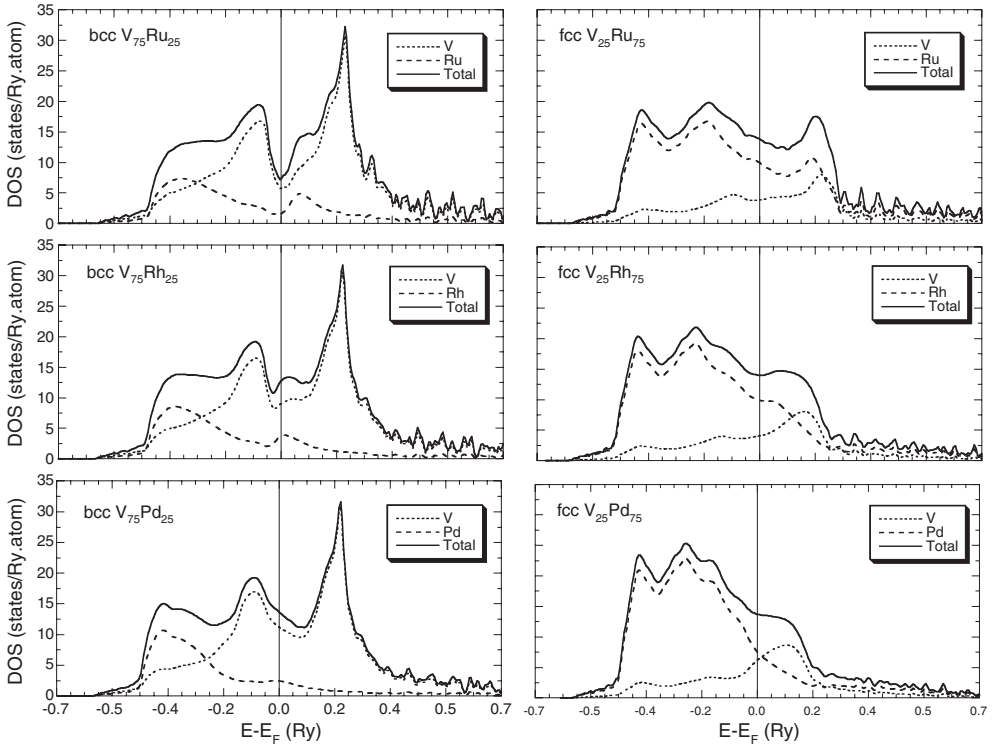

Figure 6. Total (solid curve) and partial (V: dotted, and X: dashed curves) DOS of bcc-based V_3X (left panels) and fcc-based VX_3 (right panels) alloys (X = Ru, Rh, Pd).

Ru, Rh, and Pd in this order. It has been shown that T_c peaks at $e/a = 4.7$ and 6.5 occur for solid solutions of transition metals [17]. Therefore, since $e/a = 5$ for V, T_c should increase when going from Ru to Rh, and to Pd. This is indeed experimentally observed. Later on, Dynes and Varma [18] discussed the effect of disorder on T_c by considering the role of $n(E_F)$ in the relation $\lambda = n(E_F)\langle I^2\rangle/M\langle\omega^2\rangle$. Hence the decrease in DOS at the Fermi energy when going from Pd to Rh and Ru should result in a decrease in T_c, and this is indeed observed experimentally. Moreover, the increase of Θ_D with an increase in disorder for V–X contributes to a decrease of T_c. Finally, the spin fluctuations that are of importance in dilute-Pd alloys will 'break' the Cooper pairs and enhance the decrease in T_c.

5.2. Ordered phases

The differences in the constitution phase diagrams for the three systems are reflected in the γ and Θ_D values. In the V–Rh system, three low γ values are observed for the A15, α-VIr and $L1_2$ ordered structures (at stoichiometry), whereas the highest γ value is reached for the V_3Rh_5 compound. In contrast, no drastic change is observed for the V–Pd system, the minimum γ value being reached for the $C11_b$ ordered structure of $MoPt_2$-type. One high value of γ near the stoichiometric compound VRu in the distorted B2-ordered structure is the main feature of the V–Ru system. In addition, for every alloy composition where the same type of order exists, i.e., A15, $L1_0$, and $L1_2$, γ increases when Pd replaces Rh in V. All these features reemphasize the impact of the type of order on the electronic properties.

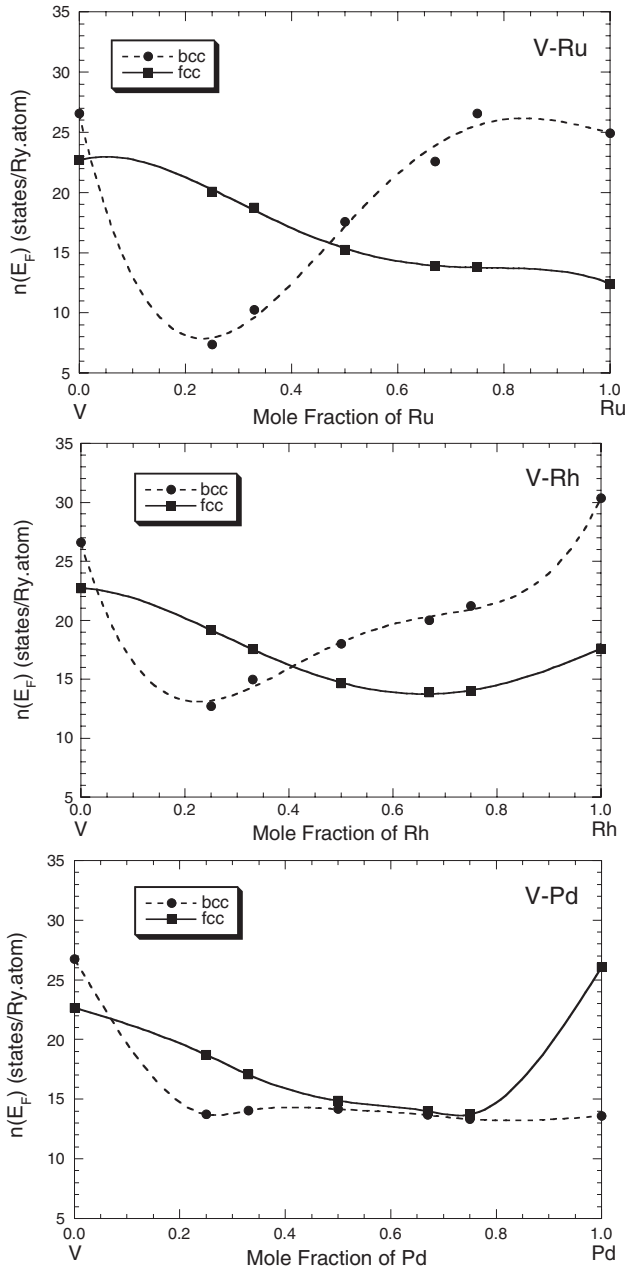

Figure 7. Variation of the DOS at the Fermi energy, $n(E_F)$, as a function of alloy composition for the V–Ru, V–Rh, and V–Pd systems based on the bcc (dashed curve and circles), and fcc (solid curve and squares) lattices.

Similarities among the variation of γ and Θ_D with alloy composition for these three systems are worth noting. Off-stoichiometry in a given system yields an increase of γ due to a disorder effect: this is the case for VRh_3 ($L1_2$), VRh ($L1_0$), and V_3Rh ($L1_2$). The case of V–Ru is rather different since a structural transformation takes place. A second similarity concerns the decrease of γ associated with an increase in chemical order at fixed alloy composition. This

appears clearly in the V–Pd system for which the disorder can be retained by quenching or cold working. For the V–Ru system, no order–disorder transformation has been observed, and therefore no disorder can be reached by classical methods. As indicated in the previous section, cold working may introduce lattice distortions. Chu *et al* [19] have noted that all strained powder samples show a bcc structure for $V_{1-c}Ru_c$ in the composition range $0.46 \leqslant c \leqslant 0.61$. Annealing in vacuum at about 950 °C for 36 h restored the ordered B2 structure. Moreover, Bernasson *et al* [20] observed that in the B2-phase region annealing of the powder at 800 °C yields a complete change of the NMR spectra. From our results shown in figure 4, it appears that in the solid-solution composition range γ depends on the heat treatment (quenching from 1100 °C for our samples, and no treatment for Bernasson's samples). This is interpreted as an indication of chemical short-range order (SRO) that seems to produce a decrease in γ. When a composition of about 25 at.% Ru is reached, long-range order (LRO) seems to appear (note that $\gamma_{\text{order}} \gg \gamma_{\text{anneal}}$), and is observed up to 48 at.% Ru, the highest composition of Ru that has been studied.

5.3. Stability and ordering trends

The trajectory of the first- and second-nearest EPIs that are functions of alloy composition are reported in the ground-state map for both the fcc and bcc cases [12] displayed in figure 8. Ordering trends are predicted for all three fcc-based alloys. More specifically, for V–Ru alloys, $L1_2$ for V_3Ru, A_2B_2-type for VRu and $D0_{22}$ for VRu_3 and VRu_5, the last three belonging to the (1 1/2 0) family of ordered states, are predicted. For V–Rh and V–Pd alloys, the (1 0 0) family of ordered states, i.e., $L1_2$ for V_3Rh (V_3Pd) and VRh_3 (VPd_3) and $L1_0$ for VRh (VPd), is predicted. By including in the ground-state analysis EPIs up to the fourth neighbours, the results are unchanged except for VPd_3, for which case the $D0_{22}$ is found to be more stable than $L1_2$. In the case of bcc-based alloys, the difference in the trends is more noticeable. Indeed, for the V–Ru and V–Rh alloys, the (1 0 0) family of ordered states, i.e., $D0_3$ for V_3Ru (V_3Rh) and VRh_3, and B2 for VRu (VRh). On the other hand, for the major stoichiometries V–Pd displays a tendency towards phase separation. The predicted ground states together with the values of the EPIs and the use of equation (4.1) allow us to predict the magnitude of the ordering energy. The variation of the mixing energy, see equation (4.2), with alloy composition together with the ordering energy in the fcc and bcc cases, see equation (4.3), provides the phase diagram of each alloy at $T = 0$ K, as shown in figure 9. From this study it can be concluded that, as observed experimentally, the alloys with a high (low) content in vanadium should be based on the bcc (fcc) lattice. In addition, the only ordered states that remain are $D0_3$ (V_3Ru), B2 (VRu), $D0_{22}$ (VRu_3) and VRu_5 for the V–Ru alloys, $D0_3$ (V_3Rh), $L1_0$ (VRh) and $L1_2$ (VRh_3) for the V–Rh alloys, and finally, $L1_0$ (VPd) and $D0_{22}$ (VPd_3) for the V–Pd alloys. These results are compatible with what is observed experimentally. Note also that in the V–Pd case, our predictions for the formation energies of the ordered states are in good agreement with those obtained with a pseudo-potential methodology [21], considering that our approach is solely based on the knowledge of the properties of the random state of the alloy.

The difference in the number of valence electrons, ΔN (3 for Ru–V, 4 for Rh–V, and 5 for Pd–V), which is a measure of the difference in the scattering properties of the electrons, controls the strength of stability. At the same time, the concentration-average number of valence electrons $\langle N \rangle$ strongly influences the tendency towards order or phase separation. Note that, for a given alloy, the variation of $\langle N \rangle$ is simply accomplished by tuning the alloy composition. If it appears that, in the series studied in this work, the variation of ΔN and $\langle N \rangle$ leads to a steady evolution of the ordering trends, the iso-electronic series (i.e., at fixed ΔN) V–Pd, Nb–Pd, and Ta–Pd shows stronger similarities as exemplified in the phase diagrams of these alloys; see figure 1. It is interesting to mention in passing that although pure Ru

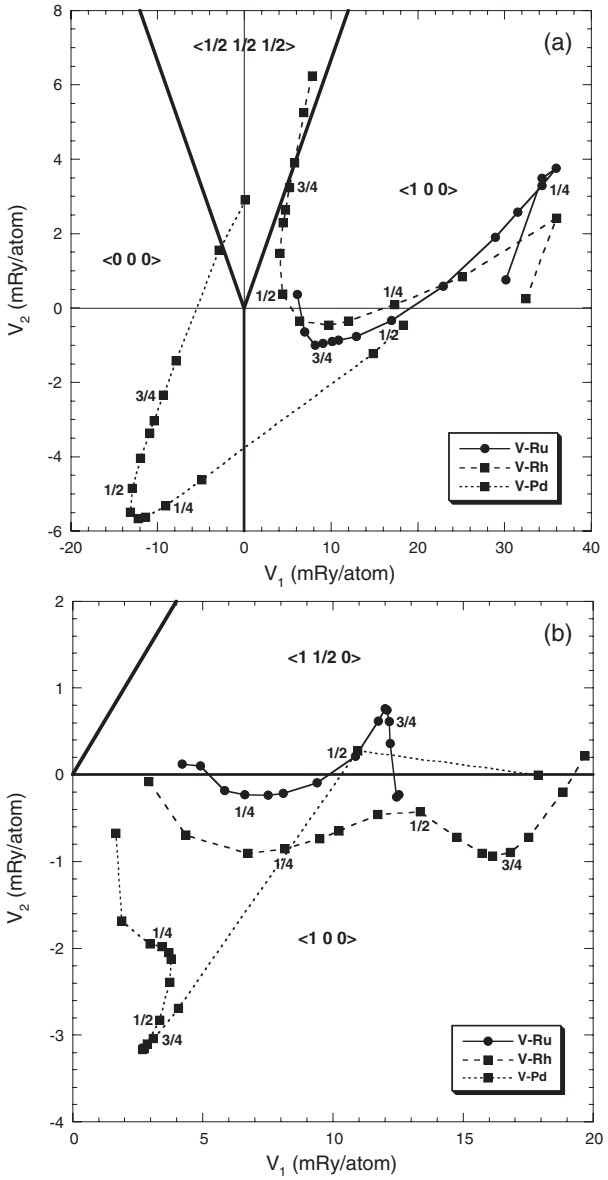

Figure 8. Variation of the effective pair interactions with alloy composition in a ground-state map representation (first versus second effective pair interaction) for V_{1-c}–X_c (X = Ru: solid curve, Rh: dashed curve, Pd: dotted curve) alloys based on the bcc (a) and fcc (b) lattices. The numbers along each curve refer to some of the stoichiometries c of the alloys.

and VRh_3 are iso-electronic ($\langle N \rangle = 8$) alloying effects clearly impact the DOS, as shown in figures 5 and 6 for these two fcc-based examples.

6. Conclusion

The relation between constitution (phase) diagrams and electronic properties for the three systems V–X (X = Ru, Rh, Pd) and the variation in the difference in the numbers of valence

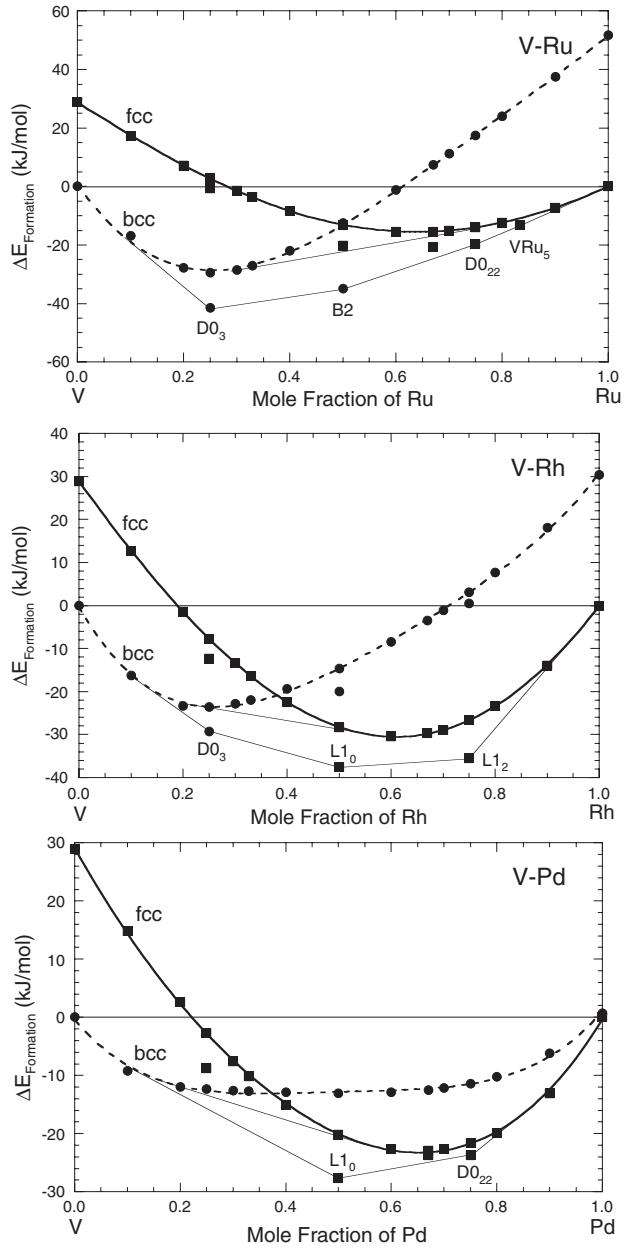

Figure 9. Variation of the formation energy of the disordered state as a function of alloy composition for the V–Ru, V–Rh, and V–Pd systems based on the bcc (dashed curve and circles), and fcc (solid curve and squares) lattices. Configuration energies of the most likely ground states have also been reported.

electrons ΔN is explained by electronic structure modelling and applications of alloy theory. A correlation has been established between the existence of ordered structures and their stability with an increase in ΔN. However, as is the case for V–Pd (for which Pd has the highest Stoner factor), spin fluctuation effects may complicate this simple conclusion.

The existence of pseudo-gaps in the density of states in the vicinity of the Fermi energy, as shown by low temperature specific heat measurements, is particularly clear for V_3Ru and VRh_3. The theory of stability confirms this feature and predicts all the ordered structures based on the fcc lattice correctly. For low ΔN, as in the case of the V–Ru system, a slightly different situation appears since the only observed ordered structure undergoes a structural transformation at low temperature. These facts reflect the high degree of instability of the B2 ordered structure around equi-atomic composition in this alloy, which in turn translates into superconducting properties and high γ values. The theoretical modelling indicates that the ordering tendencies should be rather weak for V–Ru.

Finally, the variation of the density of states at the Fermi energy with alloy composition explains overall the experimentally deduced variation of the electronic coefficient of specific heat for the three alloys considered in this work.

Acknowledgments

The work of PT has been performed under the auspices of the US Department of Energy by the University of California Lawrence Livermore National Laboratory under contract No W-7405-ENG-48. The work of VD and JK was carried out within the project AV0Z1-010-914 of the Academy of Sciences of the Czech Republic, and supported by the Grant Agency of the Academy of Sciences of the Czech Republic (Project A1010203).

References

[1] Kuentzler R and Waterstrat R M 1985 *J. Less-Common Met.* **120** 317
[2] Waterstrat R M and Manuszewski R C 1976 *J. Less-Common Met.* **48** 151
[3] Waterstrat R M and Manuszewski R C 1977 *J. Less-Common Met.* **52** 293
[4] Massalski T B (ed) 1990 *Binary Alloy Phase Diagrams* vol 1–3 (Materials Park, OH: ASM International)
[5] Waterstrat R M 2003 *J. Phase Equilib.* **24** 328
[6] Onishi N, Onozuka T and Hirabayashi M 1991 *J. Mater. Sci.* **26** 2219
[7] Kuentzler R 1970 *Thesis* University of Strasbourg, unpublished
[8] Turek I, Drchal V, Kudrnovský J, Šob M and Weinberger P 1997 *Electronic Structure of Disordered Alloys, Surfaces and Interfaces* (Boston, MA: Kluwer)
[9] Ceperley D M and Alder B J 1980 *Phys. Rev. Lett.* **45** 566
[10] Perdew J P and Zunger A 1981 *Phys. Rev.* B **23** 5048
[11] Ducastelle F and Gautier F 1976 *J. Phys. F: Met. Phys.* **6** 2039
[12] Ducastelle F 1991 *Order and Phase Stability in Alloys* (*Cohesion and Structure Series* vol 3) ed F R de Boer and D G Pettifor (Amsterdam: North-Holland)
[13] Turchi P E A 1995 *Intermetallic Compounds: Principles and Practice* vol 1, ed J H Westbrook and R L Fleischer (New York: Wiley) chapter 2, pp 21–54
[14] Obermann A, Wanzl W, Mahnig M and Wieke E 1976 *J. Less Common Met.* **49** 75
[15] Flükiger R, Heiniger F and Muller J 1969 *Proc. LT11* p 1017
[16] Asada T and Terakura K 1979 *J. Phys. Soc. Japan* **47** 1495
[17] Vonsovsky S V, Izyumov Yu A and Kurmaev E Z 1982 *Superconductivity in Transition Metals* (New York: Springer)
[18] Dynes R C and Varma C M 1976 *J. Phys. F: Met. Phys.* **6** L215
[19] Chu C H, Bucher E, Cooper A S and Maita J P 1971 *Phys. Rev.* B **4** 320
[20] Bernasson M, Descouts P, Page W L and Prina R 1971 *J. Phys. F: Met. Phys.* **1** 334
[21] Hirschl R, Hafner J and Jeanvoine Y 2001 *J. Phys.: Condens. Matter* **13** 3545